







CHEMISTRY

Water molecules bonded to the carboxylate groups at the inorganic–organic interface of an inorganic nanocrystal coated with alkanolate ligands

Jiongzhaoli Li [†], Weicheng Cao [†], Yufei Shu[†], Haibing Zhang, Xudong Qian , Xueqian Kong ^{*}, Linjun Wang ^{*} and Xiaogang Peng ^{*}

ABSTRACT

High-quality colloidal nanocrystals are commonly synthesized in hydrocarbon solvents with alkanolates as the most common organic ligand. Water molecules with an approximately equal number of surface alkanolate ligands are identified at the inorganic–organic interface for all types of colloidal nanocrystals studied, and investigated quantitatively using CdSe nanocrystals as the model system. Carboxylate ligands are coordinated to the surface metal ions and the first monolayer of water molecules is found to bond to the carboxylate groups of alkanolate ligands through hydrogen bonds. Additional monolayer(s) of water molecules can further be adsorbed through hydrogen bonds to the first monolayer of water molecules. The nearly ideal environment for hydrogen bonding at the inorganic–organic interface of alkanolate-coated nanocrystals helps to rapidly and stably enrich the interface-bonded water molecules, most of which are difficult to remove through vacuum treatment, thermal annealing and chemical drying. The water-enriched structure of the inorganic–organic interface of high-quality colloidal nanocrystals must be taken into account in order to understand the synthesis, processing and properties of these novel materials.

Keywords: nanocrystals, quantum dots, water, carboxylate ligands, interface

INTRODUCTION

Colloidal inorganic nanocrystals, including semiconductor nanocrystals with sizes in the quantum-confinement regime (quantum dots, QDs), are nanometer-sized fragments of the corresponding bulk single crystal stabilized with a monolayer of organic ligands [1]. Surface ligands affect nearly all aspects of colloidal nanocrystals, such as function, solution processibility and synthesis [2]. For instance, colloidal QDs are widely explored in high-performance display technologies [3], bio-medical diagnostics [4,5], photocatalysis [6,7] and photovoltaic devices [8–10], each of which requires specifically tailored ligands. Effects of the ligand monolayer on the synthetic chemistry of high-quality colloidal nanocrystals are well known, especially those performed in non-aqueous solvents [11–22]. The solubility of colloidal nanocrystals can be boosted by 2–6 orders of magnitude by introducing entropic

ligands [18]; this is needed for the fabrication of solution-processed optoelectronic devices.

The molecular picture of the ligand monolayer on a colloidal nanocrystal is ambiguous, especially at the interface between the inorganic nanocrystal and its organic ligands (inorganic–organic interface). High-quality nanocrystals synthesized in non-aqueous solutions are usually single crystalline in nature, and thus the interior inorganic structure can be well characterized using diffraction techniques and transmission electron microscopy [23,24]. In most cases, the composition and molecular structure of organic ligands are not too difficult to clarify [25–27]. Since 2001 [12], fatty acids and their metal salts have become the most common ligands for synthesis of high-quality nanocrystals, with their carboxylate groups bonded onto the surface metal sites of a nanocrystal. With sufficient configurational entropy from their flexible hydrocarbon chains, the alkanolate monolayer on a nanocrystal provides

Zhejiang Key Laboratory of Excited-State Materials, Department of Chemistry, Zhejiang University, Hangzhou 310027, China

*Corresponding authors.

E-mails: kxq@zju.edu.cn; ljwang@zju.edu.cn; xpeng@zju.edu.cn

[†]Equally contributed to this work.

Received 23

December 2020;

Revised 1 July 2021;

Accepted 14 July

2021

a hydrophobic outer surface region to ensure desirable solution dispersity in non-polar solvents for both synthesis and processing [18,28].

At the inorganic–organic interface, the situation is rather complex. It is evidently a transition zone with multi-functions i.e. from randomly packed and flexible organic phase to crystalline inorganic phase, from covalently bonded hydrocarbon chains to nearly ionic inorganic crystals, and from a hydrophobic and non-polar region to a strongly polar and hydrophilic region. For the most common ligand systems, i.e. fatty acid/fatty acid salts, chemical bonding between the surface metal sites and carboxylate groups has been extensively studied experimentally and theoretically [27,29,30]. As for the hydrophilic environment around the interface, there is not much knowledge.

Theoretical analysis suggested the existence of negatively charged OH^- groups at the interface for PbS QDs coated with alkanolate ligands, though the measurements were brief [30]. It was identified that, at the interface of InP QDs, there might be various forms of indium oxide species [17,31]. Synthesis of different types of high-quality oxide nanocrystals was found to be possible by simply heating up the corresponding metal fatty acid salts in hydrocarbon solvents, such as octadecene [13,14,32]. After dehydrogenation of octadecene by sodium metal, hydrolysis of indium carboxylates with trace amounts of residual water molecules occurred readily to form high-quality In_2O_3 nanocrystals [32], implying a strong capability of enriching water at the interface for continuous growth of the nanocrystals. It was suspected that there might be some water-related variation of emission properties of CdSe/CdS core/shell QDs [33,34].

Based on the facts discussed in the above paragraph, we hypothesize that there should be some water molecules adsorbed at the inorganic–organic interface for inorganic nanocrystals with carboxylate ligands. Because the commonly applied characterization methods for colloidal nanocrystals are insensitive to water and contamination is generally not carefully avoided, such water molecules have yet to be studied. Here, coupled with chemical means and computational efforts, Fourier transform infrared (FTIR) spectroscopy and nuclear magnetic resonance (NMR) spectroscopy methods with isotope labeling are developed to circumvent the hurdles of characterization. Results reveal that, on average, there is ~ 1 monolayer of water molecules at the inorganic–organic interface of different types of nanocrystals coated with alkanolate ligands, which are mostly bonded to the carboxylate groups with hydrogen bonds, instead of directly onto the inorganic surface sites.

RESULTS AND DISCUSSION

CdSe QDs as the model system

Nearly monodisperse CdSe QDs in zinc-blende structure with alkanolate ligands are applied as the main model system, and are synthesized in octadecene, with cadmium alkanolates (with excess fatty acids) and selenium powder as the precursors (see Experimental Section in supporting information for detail) [35]. Their size-dependent optical properties (see Fig. 1a, for example) can be applied as convenient probes for determining size, size distribution and concentration of the nanocrystals. Specifically, the average size is determined using the absorption peak, its sharpness offers information about their size distribution, and the QD concentration is determined using their known extinction coefficients [36]. Though CdSe QDs with different sizes are studied, results below shall be based on the QDs with a diameter of 3 nm and their first excitonic absorption peak at 550 nm (Fig. 1a) unless otherwise stated.

CdSe QDs are purified thoroughly using a literature procedure with slight modifications [36]. Briefly, the as-synthesized QDs with stearate ligands are reacted with capric acids to offer excellent dispersity in any non-polar solvents at room temperature. Multiple cycles of dissolution/precipitation are carried out to remove any unreacted metal carboxylates and free fatty acids. Previous studies identified bonding configurations of carboxylates to the surface cadmium sites [27], and therefore offer a needed reference for understanding incorporation of water molecules at the interface.

O–H vibration from the molecules at the inorganic–organic interface of CdSe QDs

Figure 1b illustrates FTIR spectra of the purified CdSe QDs dissolved in CCl_4 (labeled as Pristine CdSe in Fig. 1b), and shows strong yet broad infrared (IR) absorption between $3000\text{--}4000\text{ cm}^{-1}$. In comparison, the trace amount of water in the solvent (CCl_4) shows two sharp vibration peaks for free water at 3630 cm^{-1} (symmetric) and 3710 cm^{-1} (asymmetric) in the spectral range (Fig. S1, Supplementary Data). In addition to two sharp peaks with relatively low absorbance, the very broad and strong peak between $3200\text{--}3580\text{ cm}^{-1}$ should be associated with bonded water and/or other species with O–H vibration motif, such as neutral methanol molecules and the negatively charged hydroxyl groups (OH^-) bonded onto the surface Pb sites for PbS QDs [30]. To verify this assignment, Pristine CdSe QDs are allowed to react with a large excess of deuterium oxide (D_2O) added on top of the CCl_4 solution as

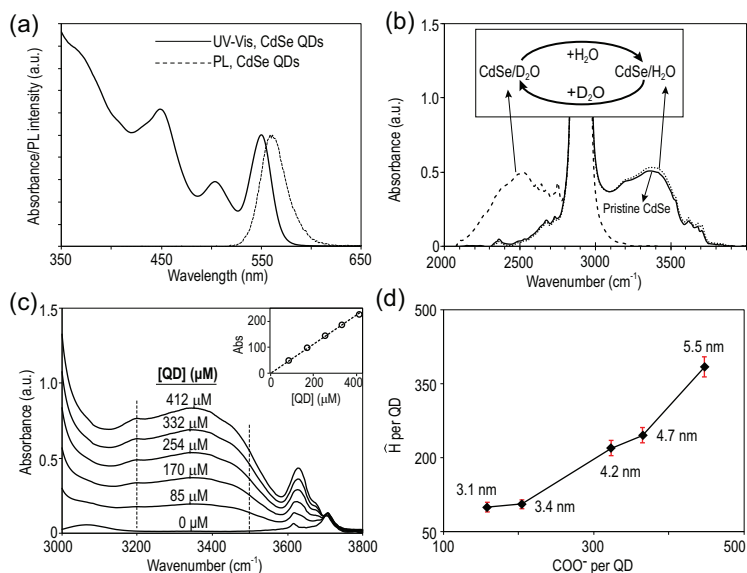


Figure 1. (a) UV–Vis and photoluminescence (PL) spectra of CdSe QDs with alkanolate ligands. (b) FTIR spectra of CdSe QDs with water and deuterium oxide treatments. ‘Pristine CdSe’ refers to the CdSe QDs before any H₂O/D₂O treatments. (c) FTIR spectra of CdSe QDs with concentration range between 0 μM and 412 μM. Inset: integrated FTIR absorbance between 3200 cm⁻¹ and 3500 cm⁻¹ versus the QD concentration. (d) Number of hydrogen atoms in hydroxy groups versus number of carboxylates per CdSe QD with different sizes.

a separate phase at room temperature. Under such conditions, it is well known that active hydrogens in the form of O–H groups can readily go through hydrogen–deuterium exchange. After removal of the D₂O layer, FTIR measurements of the exchanged QDs (labeled as ‘CdSe/D₂O’ in Fig. 1b) in the CCl₄ phase reveal that the entire broad and strong IR band above 3000 cm⁻¹ disappears while the C–H vibration band of the ligands between ~2800–3000 cm⁻¹ remains. Simultaneously, a broad and strong IR band appears between 2200–2800 cm⁻¹ for the exchanged QDs, in good accordance with O–D vibrations (Fig. S1, Supplementary Data). Figure 1b further shows that this H–D exchange process is fully reversible by reacting CdSe/D₂O with H₂O (the recovered QDs being labeled as ‘CdSe/H₂O’ in Fig. 1b).

Figure 1c demonstrates a series of FTIR spectra of the CdSe QDs with different QD concentrations in CCl₄. While absorbance of the sharp IR peak at 3710 cm⁻¹ associated with free water in the solution remains constant, absorbance of the broad IR band and some of the sharp IR peaks all increase upon increasing the QD concentration in the solution. We choose the integrated absorbance between 3200–3500 cm⁻¹ as the quantitative measure for the O–H vibrations of the interface-bonded species, which avoids possible overlapping with the C–H vibrations below

~2800–3000 cm⁻¹ and residual sharp IR peaks above 3500 cm⁻¹ from the free water molecules in the solution. For convenience, the O–H vibration motif shall be denoted as ‘active hydrogen atom (\hat{H})’ for short, referring to those that can be efficiently exchanged with deuterium atoms.

As shown in the inset of Fig. 1c, the integrated absorbance between 3200–3500 cm⁻¹ is strictly proportional to the QD concentration in the solution, implying direct association of the broad IR band with the QDs. This conclusion is further supported by Fig. 1d, which reveals that the number of active hydrogen atoms (\hat{H}) per QD increases monotonically as the size of CdSe QDs increases. Methods for quantifying the absolute number of \hat{H} per QD shall be introduced below.

Nature of the O–H motif

NMR measurements (Fig. 2a) reveal that, in addition to the broad ¹H NMR signals of alkanolate ligands, a broad ¹H NMR signal appears at ~2.57 ppm for the QDs in CDCl₃, which is consistent with the active hydrogen atoms in the form of interface-bonded molecules, either water or the negatively charged OH⁻ group. Upon addition of deuterium methanol (CD₃OD) into the CDCl₃ solution of the QDs, the broad ¹H NMR signal at ~2.57 ppm disappears. Instead, relative to the signal of hydroxyl-deuterated methanol (CH₃OD), the hydroxyl hydrogen peak of the methyl-deuterated methanol (CD₃OH) increases its intensity by ~3 times. These results confirm that there are hydroxyl species on the QD surface, which can be efficiently converted to deuterium oxide species through the hydrogen–deuterium exchange with added CD₃OD. Furthermore, the active hydrogen atoms (or surface hydroxyl groups) are not in the form of interface-bonded methanol, though methanol is applied for purification of the QDs.

Liquid-phase FTIR measurements (Fig. 2b) show that there is no free fatty acid in the solution of the purified QDs, excluding another possible form of the surface hydroxyl groups. Into this solution of QDs in dodecane, an excess amount of acryl chloride (RCOCl) is added. This completely removes the IR peak at ~1537 cm⁻¹ for asymmetric vibration of the carboxylate groups, and a few new peaks appear in the region for other types of carbonyl species in the solution, including free carboxylic acid (RCOOH), acid anhydride ((RCOO)₂O) and excess acryl chloride (Fig. 2b). Control experiments confirm that, without the purified CdSe QDs in the solution, there is no formation of either free fatty acids or acid anhydrides by addition of acryl chlorides (Fig. S2, Supplementary Data). For the current system, these

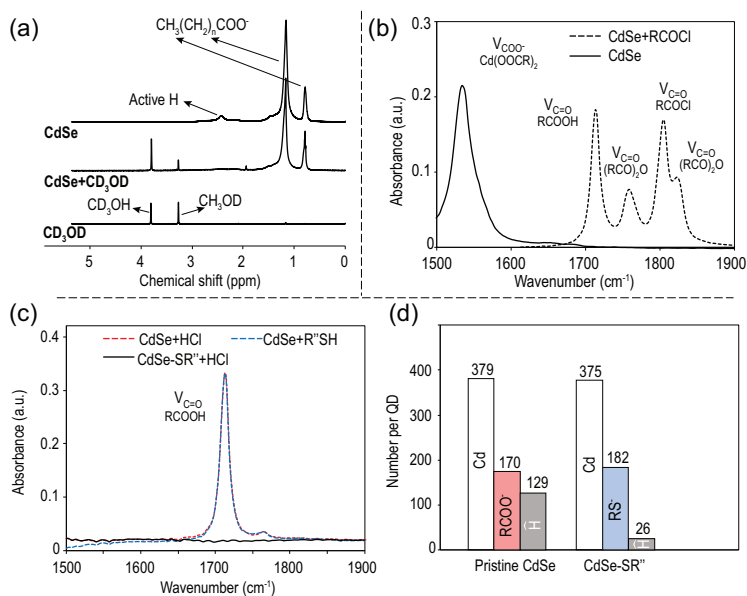
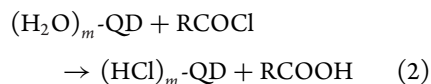
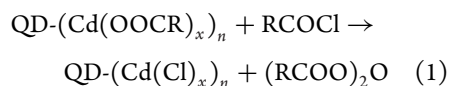


Figure 2. (a) ¹H NMR spectra of CD₃OD, CdSe QDs and CdSe QDs mixed with CD₃OD in CDCl₃. (b) FTIR spectra of CdSe QDs with/without the acyl-chloride treatment. (c) FTIR spectra of CdSe QDs reacted with HCl, reacted with thiol and reacted with HCl after the thiol treatment (with additional purification). (d) Number of atoms/molecules per QD for Pristine CdSe and thiol-coated CdSe QDs (CdSe-SR'').

products should be produced through the following reactions.



QD-(Cd(OOCR')_x)_n represents a CdSe QD with alkanolate ligands (total number of alkanolates per QD being *nx*), which reflects the fact that the carboxylate ligands are bonded with surface cadmium sites in different forms, with *x* = 0.5, 1 and 2 for (111), (100) and (110) (or other non-polar) facets, respectively [27]. Reaction between these carboxylate ligands and acryl chlorides would result in acid anhydrides (Equation (1)). After excluding the presence of methanol and carboxylic acid on the purified QDs, there are two possible reactions of acryl chlorides that yield free fatty acids from the purified QDs. Equation (2) illustrates the reaction between acryl chlorides and water molecules adsorbed on the QDs ((H₂O)_m-QD, total water molecules per QD being *m*). The other possible reaction would occur between acryl chloride and the negatively charged hydroxyl groups (OH⁻) bonded directly to the surface cadmium sites, which shall be excluded below.

Figure 2b reveals that concentrations of the resulting fatty acids and acid anhydrides are similar to each other, given IR extinction coefficients of both types of carbonyl groups being similarly high [37].

By reacting the purified CdSe QDs (Pristine CdSe) with excess HCl, all surface carboxylate ligands are converted to free fatty acids. In comparison, with the same concentration of the purified QDs, reaction between dodecanethiol (RSH) and the QDs results in an IR peak for free fatty acids with identical spectral shape and intensity (Fig. 2c). The resulting CdSe QDs coated with thiolate ligands (CdSe-SR) are purified and further reacted with HCl, which shows no IR signals in the carbonyl region (1500–1900 cm⁻¹), indicating complete replacement of the carboxylate ligands by the thiolate ones (–SR). For Pristine CdSe and CdSe-SR, the carboxylate and thiolate ligands per QD are quantified (Figs S3 and S4, Supplementary Data). The results are plotted with cadmium atoms per QD as the reference (Fig. 2d). Figure 2d also includes interface-bonded water molecules per QD for each type of QD, determined using the method in Fig. 3a (see detail in the next subsection).

Evidently, replacement of surface ligands does not affect the total number of cadmium atoms per QD, which implies a one-on-one replacement of carboxylate ligands by thiolate ligands with the same negative charge (–1). As a control experiment, thiols are confirmed to readily react with Cd(OH)₂ (Fig. S5, Supplementary Data). If there are any negatively charged hydroxyl groups bonded onto the surface cadmium sites, it should be in the form of Cd(OH)_x, and the number of thiolate ligands per CdSe-SR QD should be equal to the sum of the carboxylate and OH⁻ surface groups. Figure 2d illustrates that the number of carboxylate ligands per Pristine CdSe is equivalent to a closely packed monolayer of the ligands [36] and only ~7% less than that of the thiolate ligands per CdSe-SR QD. Because this difference is close to the overall experimental errors (3%–5% for each set of measurements) for the experiments (Fig. S4, Supplementary Data), it is reasonable to state that there are barely any negatively charged OH⁻ groups bonded on the surface of Pristine CdSe QDs. Thus, as concluded in Equation (2), the large amount of free fatty acids formed by the reaction between the Pristine CdSe QDs and acryl chlorides should solely result from the interface-bonded water molecules.

Furthermore, the results in Fig. 2c and d can be summarized by the following reactions (Equations (3) and (4)). In these reactions, both alkanolate ligands and adsorbed water molecules are presented, giving a formula for a QD as QD-(Cd(OOCR)_x)_n-(H₂O)_m. For the QDs with a specific size, it

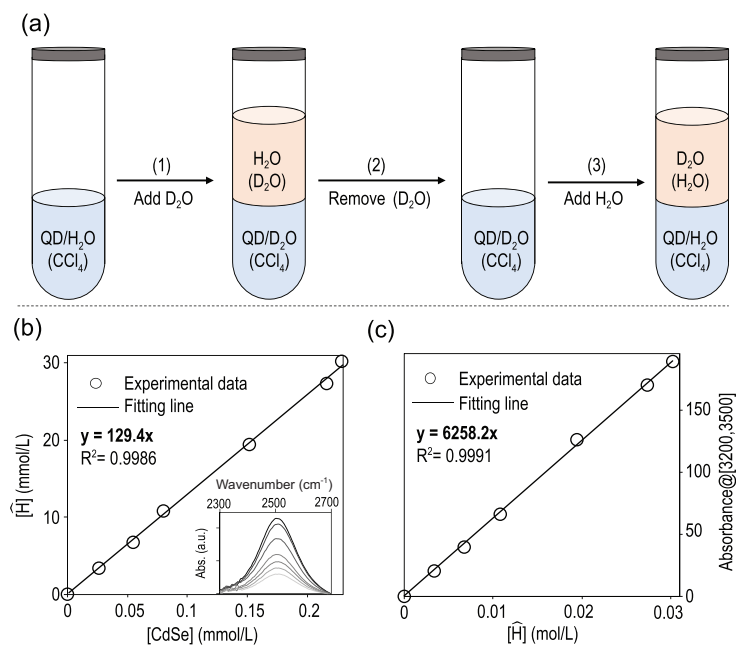
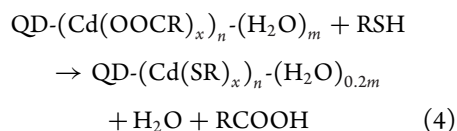
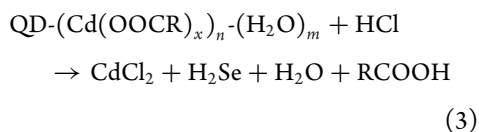


Figure 3. (a) Scheme of the hydrogen–deuterium exchange process. (b) Concentration of active hydrogen versus concentration of the QDs. Inset: FTIR spectra of D₂O in H₂O (D₂O(H₂O)) obtained by Step 3 in (a). (c) IR absorbance between 3200 cm⁻¹ and 3500 cm⁻¹ in the IR spectrum of a given sample versus concentration of active hydrogen atoms in the sample.

should be possible to calculate the stoichiometric coefficients m , x and n using the data in Figs 1d and 2d.



Interestingly, the number of water molecules decreases substantially ($\sim 80\%$) by the ligand exchange with thiolates (Fig. 2d and Equation (4)), though the number of original alkanolate ligands equals that of thiolate ligands. This suggests that the water molecules are predominately associated with the alkanolate ligands. Considering the molecular structure of the surface alkanolate ligands, one would suspect that they are most likely to appear at the hydrophilic region offered by the carboxylate groups of alkanolate ligands. Though these water molecules are neutral and should not be replaced by the negatively charged thiolate ligands, they should leave the QDs when the carboxylate groups are removed by the ligand ex-

change. Presumably, the residual water molecules ($\sim 20\%$) after the ligand exchange should be those directly bonded on the non-polar facets of the QDs, which is consistent with their low coverage of cadmium alkanolate ligands [27].

Quantitative determination of water molecules at the interface of a QD

Quantitative determination of the concentration of active hydrogen atoms in a solution is established by a hydrogen–deuterium exchange procedure (Fig. 3a). In Step 1, the purified QDs in CCl₄ are treated by a large excess of D₂O ($\sim 10^4$ in excess), which converts the surface bonded H₂O to D₂O completely (see FTIR results in Fig. 1b) through either hydrogen–deuterium exchange or H₂O–D₂O exchange. The D₂O phase with the exchanged H₂O (labeled as H₂O(D₂O)) is removed in Step 2. In Step 3, a large excess of H₂O is added onto the CCl₄ solution of the QDs with the interface-bonded D₂O, which converts the interface-bonded D₂O back to H₂O completely (see Fig. 1b). Simultaneously, the newly replaced D₂O molecules are transported into the top H₂O phase (D₂O(H₂O)). Measuring the IR spectrum of the top water phase obtained in Step 3, one would observe a characteristic IR band centered at ~ 2500 cm⁻¹ for D₂O dissolved in H₂O (Fig. 3b, inset). Using the extinction coefficients of D₂O in H₂O measured separately (Fig. S6, Supplementary Data), one can then determine the concentration of active hydrogen atoms of the interface-bonded H₂O for a specific sample [38,39].

For the typical CdSe QDs (3.0 nm in size), a series of FTIR spectra are obtained using the method outlined above for the CCl₄ solutions with different concentrations of QDs. Figure 3b plots the concentration of active hydrogen atoms versus the QD concentration in a specific solution, with the corresponding FTIR spectra summarized in Fig. 3b (inset). Results in Fig. 3b yield an excellent linear function and the slope is the number of active hydrogen atoms per Pristine QD. Specifically, each QD bonds 130 active hydrogen atoms at its inorganic–organic interface on average, corresponding to 65 water molecules at the inorganic–organic interface per CdSe QD (3.0 nm in size).

Determination of the concentration of interface-bonded water further allows measurement of the extinction coefficient of the related IR band. After measuring a series of FTIR spectra of Pristine CdSe QDs with known concentrations (see Fig. 1c for example), the integrated absorbance between 3200 and 3500 cm⁻¹ is plotted against the concentration of

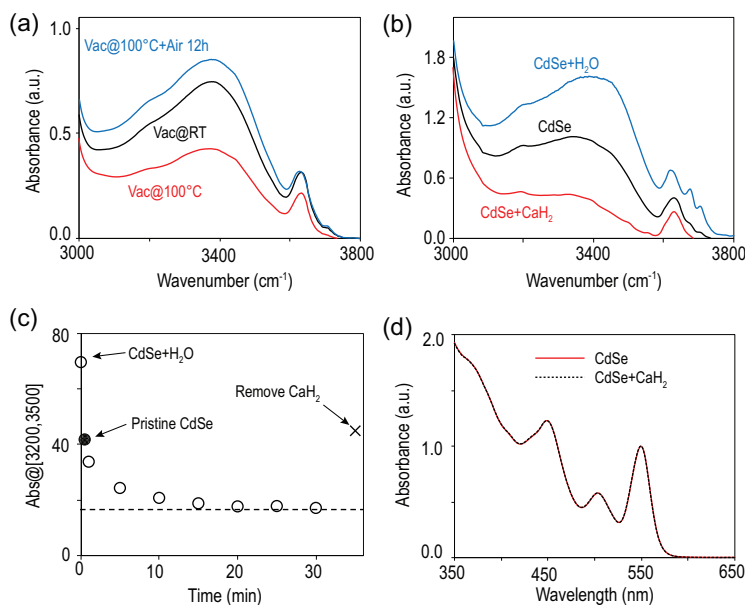


Figure 4. (a) FTIR spectra of CdSe QDs under vacuum at room temperature (Vac@RT), at 100°C for 4 hours (Vac@100°C) and re-exposed to air for 12 hours (Vac@100°C + Air 12h). (b) FTIR spectra of the freshly synthesized and purified CdSe QDs (fresh CdSe), and the QDs equilibrated with the water-saturated CCl₄ solution (CdSe + H₂O) and CaH₂-treated (CdSe + CaH₂). (c) Temporal evolution of absorbance between 3200 cm⁻¹ and 3500 cm⁻¹ during CaH₂ treatment, with data points for two control experiments. (d) UV-Vis spectra of CdSe QDs before and after CaH₂ treatment.

the active hydrogen atoms of the interface-bonded water, resulting in an excellent linear function, with the slope as the molar extinction coefficient of the active hydrogen atoms in the interface-bonded water molecules, namely, 6258 (cm L/mol) between 3200 and 3500 cm⁻¹. This provides a convenient probe for determining the number of interface-bonded water molecules per nanocrystal.

Responses of interface-bonded water molecules to environment change

After purification, the QDs in powder form are placed in a vacuum oven. At room temperature, vacuum treatment can only reduce interface-bonded water molecules by ~10% (Fig. 4a). With vacuum treatment at 100°C, the interface-bonded water molecules plateau at ~50% of that of purified QDs (Fig. 4a). The samples after the vacuum treatments recover their water content effectively by exposure to air. These results reveal that the water molecules at the inorganic–organic interface are bonded quite strongly.

After equilibrium with the water phase on top of the CCl₄ solution of QDs (see Fig. 3a for experimental set-up), absorbance of two sharp IR peaks for free water molecules in the CCl₄ solution at 3630

and 3710 cm⁻¹ increases significantly (Fig. 4b), consistent with saturation of water in CCl₄. Simultaneously, the broad IR band related to the interface-bonded water molecules of the QDs in the CCl₄ phase also increases its absorbance. In general, the number of interface-bonded water molecules on the freshly prepared CdSe QDs (Pristine CdSe QDs) varies somewhat while that of the QDs equilibrated with the water-saturated CCl₄ is rather constant. After removal of the top water phase, the number of interface-bonded water molecules remains unchanged upon exposure to air for a long period of time. Usually, the number of interface-bonded water molecules on freshly prepared QDs is 60 ± 15% of that on the QDs equilibrated with the water-saturated CCl₄.

Figure 4b shows that the addition of CaH₂ powder into the CCl₄ solution eliminates the two sharp vibration peaks of free water at 3630 and 3710 cm⁻¹ efficiently. As expected, removal of the dissolved water in the CCl₄ solution via reaction with CaH₂ noticeably reduces the number of interface-bonded water molecules on the QDs dispersed in the solution. Interestingly, the relatively broad peak at ~3630 cm⁻¹ remains strong, indicating that this peak is likely associated with one type of bonded water molecule at the inorganic–organic interface of the QDs.

CaH₂ is insoluble in CCl₄. Thus, it takes ~10 minutes for CaH₂ powder to reduce the number of water molecules at the interface per QD to a plateau (Fig. 4c). The plateau is approximately 40%–50% of that for the fresh CdSe QDs and ~30% of that for the QDs equilibrated with water-saturated CCl₄. Upon removal of CaH₂ powder from the bottom of the solution, the number of interface-bonded water molecules per QD would quickly recover to a level similar to that of the fresh CdSe QDs in CCl₄ (the point labeled as a cross in Fig. 4c), indicating the outstanding capability of water enrichment of the QDs with alkanolate ligands. Across all treatments associated with Fig. 4, the UV-Vis spectra of the QDs remain identical (Fig. 4d), indicating no influence on the inorganic core of the QDs.

Bonding configuration of interface-bonded water molecules

Typically, solid-state NMR signals of alkanolate ligands dominate the ¹H spectrum. To minimize ¹H signals of the aliphatic components, an ¹H magic-angle spinning (MAS) spectrum (Fig. 5a) is collected using the CdSe QDs coated with 98% deuterated myristate ligands, denoted as QD-My(d₂₇). Compared with the ¹H signal of the QDs coated

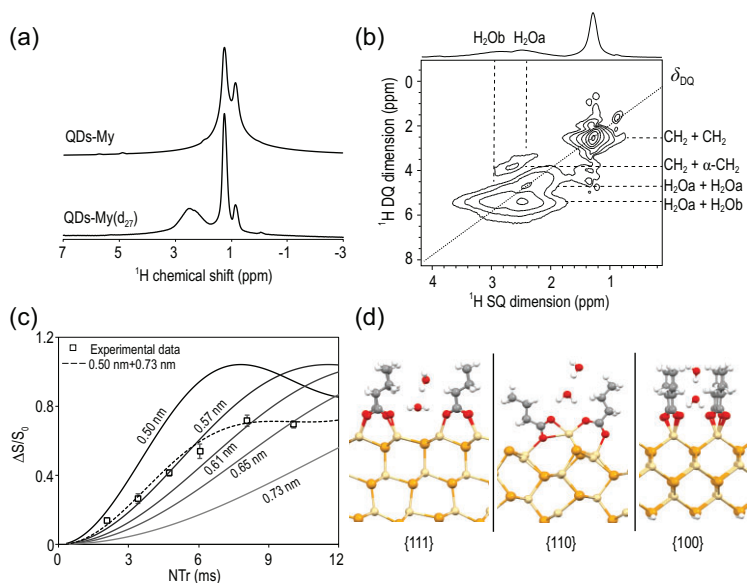


Figure 5. (a) Solid-state ^1H MAS NMR spectra of CdSe QD-My and QD-My(d_{27}). (b) DQ-SQ ^1H - ^1H homonuclear two-dimensional correlation spectra of CdSe QD-My(d_{27}). (c) REDOR curves ($\Delta S/S_0$) of the peak corresponding to water molecules and the calculated curves of different ^1H - ^{113}Cd inter-nuclear distances. As labeled, the solid lines are calculated curves for specific single distances and the dashed line is the curve for two mixed distances. (d) Optimized structures of {111}, {110} and {100} facets with two water molecules in the supercell of the slab. The Monkhorst-Pack k-point sampling was generated with a $3 \times 3 \times 1$ grid.

with regular (or protonated) myristate ligands (denoted as QD-My in Fig. 5a), the signals at 0.9 ppm (for CH_3) and 1.2 ppm (for CH_2) of QD-My(d_{27}) (with 2% remaining protons) are significantly reduced and narrowed due to reduction of proton spin populations and their dipolar couplings. Evidently, a broad ^1H peak emerges in the range between ~ 1.5 and ~ 3.5 ppm for the QD-My(d_{27}) sample, which cannot be attributed to the myristate ligands and is consistent with the ^1H of the interface-bonded water (see Fig. 2a). It was reported that the chemical shift of H_2O in a non-polar environment can be dramatically smaller than that in an aqueous environment, which has often been observed in a number of nano-complex systems and surface structures [40–42].

Double quantum-single quantum (DQ-SQ) correlation experiments are performed on QD-My(d_{27}) to probe different contributions to the emerged ^1H peak through ^1H - ^1H dipolar couplings. The DQ-SQ spectrum gives the double quantum frequency (δ_{DQ}) along the y axis, which is the sum of single quantum chemical shifts ($\delta_{\text{SQ},1} + \delta_{\text{SQ},2}$) for two coupled spin 1 and spin 2 (Fig. 5b). With the coupling information, we can distinguish different proton species and identify those in spatial proximity. The DQ dimension in Fig. 5b distinguishes

four coupling schemes including $\delta_{\text{DQ}} = 2.4$ ppm ($1.2 + 1.2$ ppm), $\delta_{\text{DQ}} = 4$ ppm ($1.2 + 2.8$ ppm), $\delta_{\text{DQ}} = 4.8$ ppm ($2.4 + 2.4$ ppm) and $\delta_{\text{DQ}} = 5.5$ ppm ($3.0 + 2.5$ ppm). The $\delta_{\text{DQ}} = 2.4$ ppm signal arises from the self-coupling of intramolecular CH_2 groups ($\delta_{\text{SQ}} = 1.2$ ppm) on the alkyl chain. The $\delta_{\text{DQ}} = 4$ ppm signal with low intensity is attributed to the $\alpha\text{-CH}_2$ ($\delta_{\text{SQ}} = 2.8$ ppm) of the myristate, which is coupled to intramolecular CH_2 ($\delta_{\text{SQ}} = 1.2$ ppm). The $\delta_{\text{DQ}} = 4.8$ and 5.5 ppm signals can be attributed to two different bonding environments of water species A and B with chemical shifts $\delta_{\text{SQ}} = 2.4$ and 3 ppm, respectively. The $\delta_{\text{DQ}} = 4.8$ ppm is the self-correlation water species A, and the $\delta_{\text{DQ}} = 5.5$ ppm is the inter-correlation between water species A and B.

In summary, the solid-state NMR measurements above suggest that the interface-bonded water molecules are not in a homogeneous environment. Instead, there are at least two distinguishable locations. This conclusion is evidently in good accordance with the FTIR results. As shown above, the IR band of the interface-bonded water molecules is broad and shifts significantly in the low-frequency direction of those related to the free water molecules in the solvent.

Distances between the interface-bonded water and the surface Cd sites

As summarized in Equation (4), exchange of the original alkanolate ligands by thiolate ones would largely eliminate the interface-bonded water molecules, suggesting that most of them are not directly attached to the inorganic surface. Solid-state NMR measurements can offer quantitative information on the ^1H - ^{113}Cd inter-nuclear distance between the interface-bonded water and the Cd atoms on the nanocrystal surface. This is achieved by $^1\text{H}\{^{113}\text{Cd}\}$ rotational echo double resonance (REDOR) experiments on a doubly labeled QD(^{113}Cd)-My(d_{27}) sample (Fig. 5c) [43,44].

The isotope enrichment of ^{113}Cd for CdSe QDs ensures all water molecules are coupled with their nearest Cd sites. The deuteration of myristate ligands occurs for the same reason mentioned above, i.e. to minimize the background ^1H signals of the aliphatic chain. The REDOR experiments provide two signals. The S signal is obtained when both ^1H and ^{113}Cd resonances are irradiated, and the S_0 reference signal is observed if only the ^1H resonance is irradiated. The difference between S and S_0 , i.e. ΔS , indicates the ^1H signals that are coupled to ^{113}Cd spins. The ratio of $\Delta S/S_0$ versus the periods of pulse irradiation can pro-

vide a quantitative measure of ^1H – ^{113}Cd dipolar coupling (Figs S7 and S8, Supplementary Data). For rigid molecules, the dipolar coupling is directly related to the inter-nuclear distance (Fig. 5c). It is possible that the water molecules are rotating, which would lead to a certain level of uncertainty of distance. However, by reducing the measurement temperature of REDOR from 300 K to 196 K (Figs S7 and S8, Supplementary Data), we see little difference in the $\Delta S/S_0$ curve. This suggests the water molecules are rigid relative to the inorganic surface in the time scale of REDOR measurements, and therefore the inter-nuclear distance between ^1H and ^{113}Cd can be derived.

The REDOR measurements provide an overall response for the distance between the water molecules and the ^{113}Cd spins at the inorganic–organic interface. Consistent with the other measurements discussed above, the experimental data cannot be fitted with single distance. Instead, the distance between water molecules and inorganic surface in the range of 0.5–0.7 nm can well fit the experimental data (Fig. 5c). This range means these water molecules are mostly not directly bonded to the surface sites of inorganic nanocrystals but are separated by a distance of roughly two or three chemical bonds (Table S1, Supplementary Data). To further uncover the bonding environment and facet-specific location of water molecules, we resort to detailed analysis with computational methods.

To model water adsorption at the interface of CdSe QDs, all three types of low-index facets of zincblende structure, namely $\{100\}$, $\{111\}$ and $\{110\}$, are considered. As revealed in our recent study [27], alkanolate ligands are dominantly coordinated to the surface cadmium sites on the polar $\{100\}$ and $\{111\}$ facets of CdSe nanocrystals in chelating and bridging modes, respectively. In addition, neutral cadmium-carboxylate ligands form weak coordination on the non-polar $\{110\}$ facets with a very low surface coverage. As shown in Fig. 5d, we use slab models with supercells to simulate ideal facets of CdSe nanocrystals and butyrate ligands to represent long-chain carboxylates to reduce the computational cost. On each kind of facet, one to three water molecules are considered in the supercell. The structures are optimized by density functional theory (DFT) with Quantum Espresso. The van der Waals density functional (vdW-DF) exchange-correlation function is adopted to describe electronic and hydrogen bond interactions. The plane-wave kinetic energy cutoff is set to be 60 Ry. The optimization is carried out until the forces on all atoms are lower than 0.025 eV/Å.

Figure 5d shows that, though coordination between alkanolate ligands and the inorganic surface

differs from one type of facet to another, the water molecules at the interface are bonded to the hydrophilic region—specifically carboxylate groups of alkanolate ligands—in similar forms. Instead of direct bonding to the inorganic surface, the nearest monolayer of water molecules to the inorganic surface is hydrogen-bonded to two oxygen atoms from two adjacent carboxylate groups on the surface of a nanocrystal. The oxygen atom of the nearest water molecule is further connected to a hydrogen of another water molecule that forms the second monolayer of water molecules at the interface. The bonding energy of the hydrogen bonds is found to be quite high on all three types of facets (Table S2, Supplementary Data), consistent with their stability against vacuum treatments, thermal annealing and chemical drying procedures. The average distance between the hydrogen in the interface-bonded H_2O and the surface cadmium sites on a nanocrystal is calculated to be in the range of 0.5 (the first monolayer) and 0.7 nm (the second monolayer), which fits quite well with the NMR results (Table S1, Supplementary Data).

Interface-bonded water molecules in different types of inorganic nanocrystals with alkanolate ligands

The results above suggest that it is the hydrophilic region—specifically the carboxylate groups—of the alkanolate ligands that efficiently enrich water molecules at the inorganic–organic interface through hydrogen bonds between carboxylate groups and water molecules. Upon introduction of ‘greener synthetic routes’ for colloidal nanocrystals [12], alkanolate ligands have become the most applied ligands in the synthesis of nearly all types of high-quality inorganic nanocrystals in hydrocarbon solvents. Thus, interface-bonded water might be a common structure feature for high-quality colloidal nanocrystals. Results in Fig. 6 confirm the hypothesis. Different types of colloidal nanocrystals, including CdSe/CdS core/shell QDs [45], CdS QDs [46], ZnSe QDs [47], III-V QDs (InP) [48], Fe_3O_4 nanocrystals [13,32] and In_2O_3 nanocrystals [13,32], are synthesized in the most common hydrocarbon solvent (octadecene) and with metal alkanolates (sometimes with excess fatty acids) as both cationic precursors and ligands following standard methods. FTIR measurements reveal that, for all nanocrystals studied, the number of interface-bonded water molecules is approximately in the same order of magnitude as the number of alkanolate ligands.

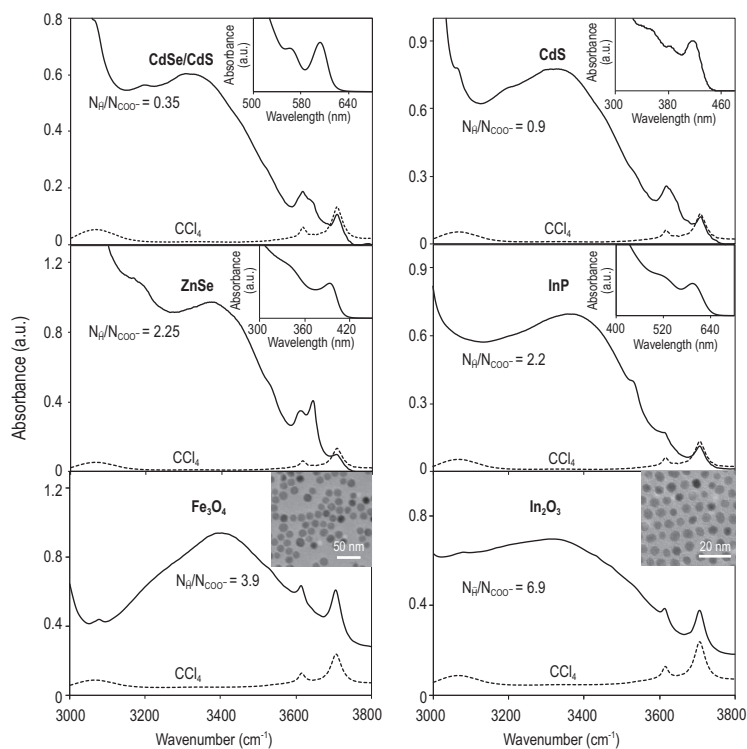


Figure 6. FTIR spectra of different types of inorganic nanocrystals coated with alkanoate ligands. FTIR spectrum of the solvent (CCl_4) is provided as a reference. Insets: the corresponding UV-Vis spectra for QDs, and TEM images for oxide nanocrystals. The ratio between the active hydrogen atoms in the form of interface-bonded water molecules and carboxylate ligands is given in each plot.

CONCLUSION AND PERSPECTIVE

In conclusion, within the inorganic–ligand interface of colloidal nanocrystals synthesized in non-aqueous solvents with alkanoate ligands, there are a large amount of bonded water molecules. These water molecules are enriched at the hydrophilic region of a colloidal nanocrystal, most of which are bonded to the carboxylate groups of the alkanoate ligands via hydrogen bonds. Results suggest that replacement of carboxylate groups through ligand exchange, such as replacing the alkanoate ligands with thiolate ligands, could dramatically decrease the number of interface-bonded water molecules. The common features of the inorganic–organic interface illustrated here open a new door not only for understanding optical, chemical, photo-chemical and photo-catalytic properties of high-quality colloidal nanocrystals, but also for designing synthetic and processing chemistry for these novel materials.

SUPPLEMENTARY DATA

Supplementary data are available at [NSR](#) online.

FUNDING

This work was supported by the Key Research and Development Program of Zhejiang Province (2020C01001) and the National Natural Science Foundation of China (21922305, 21873080 and 21703202).

AUTHOR CONTRIBUTIONS

Jiongzhao Li and Xiaogang Peng proposed and supervised the project. Yufei Shu and Xudong Qian carried out the synthesis and infrared spectroscopy tests. Weicheng Cao and Xueqian Kong carried out the NMR tests. Haibing Zhang and Linjun Wang carried out the DFT calculations. Jiongzhao Li, Yufei Shu, Weicheng Cao and Xiaogang Peng co-wrote the manuscript. All authors discussed the results and participated in analyzing the experimental results.

Conflict of interest statement. None declared.

REFERENCES

1. Brus LE. Electron–electron and electron–hole interactions in small semiconductor crystallites: the size dependence of the lowest excited electronic state. *J Chem Phys* 1984; **80**: 4403–9.
2. Yin Y and Alivisatos AP. Colloidal nanocrystal synthesis and the organic–inorganic interface. *Nature* 2005; **437**: 664–70.
3. Shu Y, Lin X and Qin H *et al.* Quantum dots for display applications. *Angew Chem Int Ed* 2020; **59**: 22312–23.
4. Bruchez M, Moronne M and Gin P *et al.* Semiconductor nanocrystals as fluorescent biological labels. *Science* 1998; **281**: 2013–6.
5. Chan WCW and Nie S. Quantum dot bioconjugates for ultrasensitive nonisotopic detection. *Science* 1998; **281**: 2016–8.
6. Han Z, Qiu F and Eisenberg R *et al.* Robust photogeneration of H_2 in water using semiconductor nanocrystals and a nickel catalyst. *Science* 2012; **338**: 1321–4.
7. Li X-B, Tung C-H and Wu L-Z. Semiconducting quantum dots for artificial photosynthesis. *Nat Rev Chem* 2018; **2**: 160–73.
8. Huynh WU, Peng X and Alivisatos AP. CdSe nanocrystal rods/poly(3-hexylthiophene) composite photovoltaic devices. *Adv Mater* 1999; **11**: 923–7.
9. Cao Y, Stavrinadis A and Lasanta T *et al.* The role of surface passivation for efficient and photostable PbS quantum dot solar cells. *Nat Energy* 2016; **1**: 16035.
10. Xu J, Voznyy O and Liu M *et al.* 2D matrix engineering for homogeneous quantum dot coupling in photovoltaic solids. *Nat Nanotechnol* 2018; **13**: 456–62.
11. Murray CB, Norris DJ and Bawendi MG. Synthesis and characterization of nearly monodisperse CdE (E = sulfur, selenium, tellurium) semiconductor nanocrystallites. *J Am Chem Soc* 1993; **115**: 8706–15.
12. Qu L, Peng ZA and Peng X. Alternative routes toward high quality CdSe nanocrystals. *Nano Lett* 2001; **1**: 333–7.
13. Jana NR, Chen Y and Peng X. Size- and shape-controlled magnetic (Cr, Mn, Fe, Co, Ni) oxide nanocrystals via a simple and general approach. *Chem Mater* 2004; **16**: 3931–5.

14. Park J, An K and Hwang Y *et al.* Ultra-large-scale syntheses of monodisperse nanocrystals. *Nat Mater* 2004; **3**: 891–5.
15. Talapin DV, Nelson JH and Shevchenko EV *et al.* Seeded growth of highly luminescent CdSe/CdS nanoheterostructures with rod and tetrapod morphologies. *Nano Lett* 2007; **7**: 2951–9.
16. Ithurria S and Dubertret B. Quasi 2D colloidal CdSe platelets with thicknesses controlled at the atomic level. *J Am Chem Soc* 2008; **130**: 16504–5.
17. Cros-Gagneux A, Delpech F and Nayral C *et al.* Surface chemistry of InP quantum dots: a comprehensive study. *J Am Chem Soc* 2010; **132**: 18147–57.
18. Yang Y, Qin H and Jiang M *et al.* Entropic ligands for nanocrystals: from unexpected solution properties to outstanding processability. *Nano Lett* 2016; **16**: 2133–8.
19. Tan R, Yuan Y and Nagaoka Y *et al.* Monodisperse hexagonal pyramidal and bipyramidal wurtzite CdSe–CdS core–shell nanocrystals. *Chem Mater* 2017; **29**: 4097–108.
20. Ghosh S and Manna L. The many ‘facets’ of halide ions in the chemistry of colloidal inorganic nanocrystals. *Chem Rev* 2018; **118**: 7804–64.
21. Hazarika A, Fedin I and Hong L *et al.* Colloidal atomic layer deposition with stationary reactant phases enables precise synthesis of ‘digital’ II–VI nanoheterostructures with exquisite control of confinement and strain. *J Am Chem Soc* 2019; **141**: 13487–96.
22. Zhu H, Fan Z and Yu L *et al.* Controlling nanoparticle orientations in the self-assembly of patchy quantum dot–gold heterostructural nanocrystals. *J Am Chem Soc* 2019; **141**: 6013–21.
23. Murray CB, Kagan CR and Bawendi MG. Synthesis and characterization of monodisperse nanocrystals and close-packed nanocrystal assemblies. *Annu Rev Mater Sci* 2000; **30**: 545–610.
24. Nasilowski M, Mahler B and Lhuillier E *et al.* Two-dimensional colloidal nanocrystals. *Chem Rev* 2016; **116**: 10934–82.
25. Hassinen A, Moreels I and De Nolf K *et al.* Short-chain alcohols strip X-type ligands and quench the luminescence of PbSe and CdSe quantum dots, acetonitrile does not. *J Am Chem Soc* 2012; **134**: 20705–12.
26. Chen PE, Anderson NC and Norman ZM *et al.* Tight binding of carboxylate, phosphonate, and carbamate anions to stoichiometric CdSe nanocrystals. *J Am Chem Soc* 2017; **139**: 3227–36.
27. Zhang J, Zhang H and Cao W *et al.* Identification of facet-dependent coordination structures of carboxylate ligands on CdSe nanocrystals. *J Am Chem Soc* 2019; **141**: 15675–83.
28. Pang Z, Zhang J and Cao W *et al.* Partitioning surface ligands on nanocrystals for maximal solubility. *Nat Commun* 2019; **10**: 2454.
29. Liu L, Zhuang Z and Xie T *et al.* Shape control of CdSe nanocrystals with zinc blende structure. *J Am Chem Soc* 2009; **131**: 16423–9.
30. Zherebetsky D, Scheele M and Zhang Y *et al.* Hydroxylation of the surface of PbS nanocrystals passivated with oleic acid. *Science* 2014; **344**: 1380–4.
31. Xie L, Harris DK and Bawendi MG *et al.* Effect of trace water on the growth of indium phosphide quantum dots. *Chem Mater* 2015; **27**: 5058–63.
32. Narayanaswamy A, Xu H and Pradhan N *et al.* Formation of nearly monodisperse In₂O₃ nanodots and oriented-attached nanoflowers: hydrolysis and alcoholysis vs pyrolysis. *J Am Chem Soc* 2006; **128**: 10310–9.
33. Cordero SR, Carson PJ and Estabrook RA *et al.* Photo-activated luminescence of CdSe quantum dot monolayers. *J Phys Chem B* 2000; **104**: 12137–42.
34. Gómez DE, van Embden J and Mulvaney P *et al.* Exciton–trion transitions in single CdSe–CdS core–shell nanocrystals. *ACS Nano* 2009; **3**: 2281–7.
35. Pu C, Zhou J and Lai R *et al.* Highly reactive, flexible yet green Se precursor for metal selenide nanocrystals: Se-octadecene suspension (Se-SUS). *Nano Res* 2013; **6**: 652–70.
36. Li J, Chen J and Shen Y *et al.* Extinction coefficient per CdE (E = Se or S) unit for zinc-blende CdE nanocrystals. *Nano Res* 2018; **11**: 3991–4004.
37. Bellamy LJ. *The Infrared Spectra of Complex Molecules*, 2nd edn. London: Chapman and Hall, UK, 1980, 128–94.
38. Shon W, Yim SP and Lee L *et al.* Advances in deuterium dioxide concentration measurement. *Fusion Eng Des* 2016; **109–11**: 398–406.
39. Park K, Kim Y and Lee KJ. Analysis of deuterated water contents using FTIR bending motion. *J Radioanal Nucl Chem* 2019; **322**: 487–93.
40. Alam TM, Liao Z and Nyman M *et al.* Insight into hydrogen bonding of uranyl hydroxide layers and capsules by use of ¹H magic-angle spinning NMR spectroscopy. *J Phys Chem C* 2016; **120**: 10675–85.
41. Trickett CA, Osborn Popp TM and Su J *et al.* Identification of the strong Brønsted acid site in a metal–organic framework solid acid catalyst. *Nat Chem* 2019; **11**: 170–6.
42. Ben Osman M, Diallo-Garcia S and Herledan V *et al.* Discrimination of surface and bulk structure of crystalline hydroxyapatite nanoparticles by NMR. *J Phys Chem C* 2015; **119**: 23008–20.
43. Gullion T and Schaefer J. Rotational-echo double-resonance NMR. *J Magn Reson* 1989; **81**: 196–200.
44. Mueller KT, Jarvie TP and Aurentz DJ *et al.* The REDOR transform: direct calculation of internuclear couplings from dipolar-dephasing NMR data. *Chem Phys Lett* 1995; **242**: 535–42.
45. Zhou J, Zhu M and Meng R *et al.* Ideal CdSe/CdS core/shell nanocrystals enabled by entropic ligands and their core size-, shell thickness-, and ligand-dependent photoluminescence properties. *J Am Chem Soc* 2017; **139**: 16556–67.
46. Yu WW and Peng X. Formation of high-quality CdS and other II–VI semiconductor nanocrystals in noncoordinating solvents: tunable reactivity of monomers. *Angew Chem Int Ed* 2002; **41**: 2368–71.
47. Lin S, Li J and Pu C *et al.* Surface and intrinsic contributions to extinction properties of ZnSe quantum dots. *Nano Res* 2020; **13**: 824–31.
48. Xu Z, Li Y and Li J *et al.* Formation of size-tunable and nearly monodisperse InP nanocrystals: chemical reactions and controlled synthesis. *Chem Mater* 2019; **31**: 5331–41.